PRE-DIFFUSION TO IMPROVE THE THERMAL FATIGUE STRENGTH OF OVERLAY COATINGS ON NICKEL-BASE SUPERALLOYS

by

CARLOS ANDRÉS ONCINA

B.S.M.E. San Diego State University (1985)

Submitted in partial fulfillment

of the requirements for the degree of

MASTER OF SCIENCE

in

MECHANICAL ENGINEERING

at the

MASSACHUSETTS INSTITUTE OF TECHNOLOGY

January 20, 1989

Signature of Author _____
Department Of Mechanical Engineering
January 20, 1989

Certified By _____
Professor Frank A. McClintock
Thesis Supervisor

Accepted By _____
Professor Ain A. Sonin
Chairman Departmental Committee on Graduate Studies

Pre-diffusion to Improve the Thermal Fatigue Strength

of Overlay Coatings on Nickel-Base Superalloys

by

Carlos A. Oncina

Submitted to the Department of Mechanical Engineering

on January 20, 1989 in partial fulfillment of the requirements

for the degree of Master of Science in

Mechanical Engineering

Abstract

The beneficial effects of pre-diffusion to impede the formation of internal (Kirkendall) voids leading to thermal fatigue of a 92 μm-thick EB-PVD coated (NiCoCrAlY) single crystal nickel-base superalloy (CMSX-3) was investigated by induction heating of a {100} stepped-disk specimen.

A 60 hour aging of the specimen at 1090 °C in air created a 20 μm β–α–γ transition zone between the coating and substrate and reduced the concentration gradient of Ni and Al through the interface to 3.0 at%/mm, which was predicted by a binary diffusion analysis to be 2.5 at%/mm. Subsequent thermal fatigue testing (comprising of 6000 thermal cycles of 6 second heating from 520 °C to 1090 °C, 60 hold, and 15 cooling to 520 °C) generated strain ranges in the coating between $\Delta\varepsilon^{mech} = 0.51\%$ at [110] and 0.71% at [100]. Micrographic examination revealed a net reduction in the gradient induced internal (Kirkendall) void formation from a mean void spacing of 110 μm in a reference specimen to 150 μm in the current specimen, and eliminated crack propagation into the substrate from these voids.

Thesis Supervisor: Dr. Frank A. McClintock

Title: Professor of Mechanical Engineering

ACKNOWLEDGEMENTS

It is with deep appreciation and a rejuvenated spirit that I e press my thanks to Professor Frank A. McClintock, for not only this thesis and all associated ıtems, but for the knowledge that such people exist.

Tc E.P. Busso for guidıng me through the technical aspects of the thesis, and along with J.W. Holmes, for laying down the groundwork. To Steve Recca, Leonard Sudenfield, Yin Lin Xie, and Don Fitzgerald for provıding the usually unheralded technical expertise which make experimental projects work. To all the officemates both at G.E. and M.I.T. who lent companionship and support.

To General Motors-Allison Turbıne Division for donatıon of the CMSX-3 material. For partial financial support for this work provided through the Natıonal Science Foundation, Grant DMR-87-10217.

To General Electric Aircraft Engine Group-Lynn for providing me the opportunity to attend M.I.T. through their ACE/ABC-program these past three-and-one-half years. To all the managers for whom I worked during this period, Bıll Blanton, Wayne Oliver, Chris Johnston and especially my current manager Ted Oldakowski.

Thank you.

CONTENTS

LIST OF TABLES

LIST OF FIGURES

1 INTRODUCTION

Advances in aircraft gas-turbine materials have resulted in the introduction of single-crystal superalloys as the material of choice for turbine blades. These nickel-base superalloys have the creep and fatigue characteristics, but lack the hot-corrosion, oxidation, and surface erosion properties required for actual service. To arrest these detrimental affects, overlay coatings such as NiCoCrAlY are applied to the surface of the turbine blades. Recent investigations by Holmes, Busso, and McClintock [1][2] have shown that the thermal fatigue produced by the mission cycle of the turbine greatly reduces its expected life compared with that expected from diffusion and steady-state oxidation. With NiCoCrAlY, the prime mechanism of failure was the formation of internal (Kirkendall) voids at the interface of the coating and substrate material, their growth by diffusion processes, and subsequent cracking from them. Diffusion of the coating before service might reduce the Kirkendall voids and improve the life of the turbine blade. This work describes tests of that hypothesis.

In order to directly validate the benefits resulting from pre-diffusion on internal (Kirkendall) void-induced cracking, a stepped-disk specimen of a single crystal nickel-base superalloy (CMSX-3), with a 92 μm thick electron-beam physical-vapor-deposited (EB-PVD) NiCoCrAlY coating as used by Busso and McClintock [2], was subjected to 6000 thermal cycles. The heating and cooling rate cycle chosen was the cycle of [2] which produced coating strain ranges between $\Delta\varepsilon^{mech} = 0.51\%$ at [110] and 0.71% [100] and led to internal (Kirkendall) void formation and subsequent cracking, but not the severe surface-initiated cracking due to tensile cooling loads. The thermal cycling of the specimen was obtained using a

heating technique developed by Holmes and McClintock [3][4] and modified by Busso and McClintock [5] for 14 mm diameter specimens.

2 EXPERIMENTAL PROCEDURE

2.1 Specimen Description

The specimens used were from the same rod of CMSX-3 (composition shown in Table 1) as used by Busso and McClintock [2]. 14 mm diameter stepped-disk specimens were machined from a mono-crystalline rod with their faces normal to the [001] preferred crystallographic growth direction and with rim thickness on the order of aircraft engine turbine trailing edges (0.9 mm). This produced specimens with cubic orientations from [100] to [110] along the periphery, as shown in Figure 1. The overlay coating was applied by an electron-beam physical-vapor-deposition (EB-PVD) process to a nominal thickness of 92 μm. The specimens used by Busso and McClintock [2] and in this study were all subjected to a heat treatment of 4 hr in vacuum at 1079 °C, and then cooled to 760 °C at a rate of 0.77 °C/s. An aging treatment for 20 hours in argon at 871 °C was then performed to further precipitate growth. A glass bead peening operation was also performed. The periphery of all the specimens had surface pits with diameters ranging from 30-70 μm.

For this investigation, determining the consequences on internal (Kirkendall) void induced cracking due to the Ni and Al concentration gradients present between the overlay coating and the substrate, a further 60 hour heat treatment at 1090 °C in air was performed. The periphery of the tested specimen had 33 surface pits (from which all subsequent cracks occurred). A discussion of the

pre-diffusion analysis performed to obtain the heat treatment time is described later in Section 3.

2.2 Coating Characteristics

The NiCoCrAlY overlay coating (composition shown in Table 1) used in this study was chosen based on a variety (of usually opposing parameters) detailed in Busso and McClintock [2] and summarized here as oxidizing operating conditions. diffusion stability, ductility and brittle-to-ductile transition temperature, and thermal expansion mismatch characteristics. With a high temperature (1090 °C) oxidizing environment, a Ni-rich alloy is better suited to withstand the operating conditions. A lower temperature (950 °C) hot-corrosion environment would suggest a Co-rich coating [6]. The Ni-rich coating is more stable on a Ni-based substrate with respect to coating-substrate interdiffusion. A Ni-rich alloy also inhibits less protective oxides of Co, Cr and Ni and promotes Al_2O_3 [7]. The need for ductility in the coating to withstand rapid cooling necessitates a low brittle-to-ductile transition temperature. This ductility comes at the expense of the oxidation and hot corrosion resistance provided by a high Al content. Finally, the thermal expansion coefficients of the coating and substrate (Figure 2) must be close to reduce the inelastic strain ranges created in the coating during thermal cycling.

2.3 Test Apparatus

A technique developed by Holmes and McClintock [3][4] using a 450 kHz induction generator was used to heat the periphery of the specimen within a few seconds and produce transient thermal strains in the specimen coating and substrate. These strains arise due to the localized heating zone (skin effect) created by induction

heating, which in turn creates a fast temperature gradient within the specimen. Details of the apparatus and modification to 14 mm diameter specimens are given in Busso and McClintock [4][5]. The main advantage of induction heating is the ease of replicating typical gas-turbine strain and temperature ranges through control of the applied heating and cooling rates and relatively simple means of determining temperature distributions through the use of appropriately positioned thermocouples, verified with an optical fiber pyrometer.

2.4 Thermal Strain History and Thermal Fatigue Test

In Busso and McClintock [2] coating strain ranges above $\Delta\varepsilon^{mech} = 0.51\%$ were shown to create internal (Kirkendall) voids and subsequent cracking. A 6 second heat, 60 second hold and 15 second cooling cycle, Figure 3, generated coating strain ranges from $\Delta\varepsilon^{mech} = 0.51\%$ to 0.71% along the periphery in the [110] to [100] directions, respectively. A comprehensive discussion of the finite element analysis used to arrive at these strains is presented by Busso and McClintock [5]. These heating and cooling times are consistent with the transient thermal conditions found in commercial and military aircraft during take-offs and landings. The 60 second hold time at 1090 °C along with forced air cooling through the center of the specimen allowed the specimen to reach typical cruise conditions (steady-state) compression in the periphery in a minimum amount of time prior to cooling. This allowed 6000 low cycle fatigue cycles to accumulate within a reasonable experimental time (approximately 1 week of continuous cycling).

3 DIFFUSION

3.1 Theory

In order to estimate the reduction in Ni and Al concentration gradient with respect to time of diffusion, Grube's method using Fick's second law [8] was used to model the coating/substrate binary system and then verified by correlation with experimental data obtained by [2]. The Grube method is only applicable to those binary systems in which the diffusivity varies slightly with composition as in the present case of the elements in the coating and substrate, which differ in composition of Ni and Al, neglecting all other components. Fick's second law can be stated in terms of the atom fraction of alloy element A, N_A, and the diffusivity $\tilde{D}$:

$$\frac{\partial N_A}{\partial t} = \frac{\partial}{\partial x} \tilde{D} \frac{\partial N_A}{\partial x} . \qquad (1)$$

The solution of Eq. 1 for a diffusion couple with the atom fractions N_A^1 and N_A^2 on either side of the interface at a distance x (mm) from it, and with constant $\tilde{D}$ is [8]:

$$N_A(x, t) = \frac{N_A^1 + N_A^2}{2} + \frac{N_A^1 - N_A^2}{2} \left(erf \frac{x}{\sqrt{\tilde{D}t}} \right), \qquad (2)$$

where the error function is defined by:

$$erf(y) = \frac{2}{\sqrt{\pi}} \int_0^y e^{-y^2} dy . \qquad (3)$$

3.2 Initial Theoretical Correlation

To test the accuracy of Eq. 2 in predicting the concentration of A in the binary system, two correlations with experimental data were performed.

The first correlation with experimental data was the solution of Eq. 2 for $\tilde{D}$ knowing the concentration of aluminum at a given time of diffusion for varying distance from the initial interface. The concentration, distance, and time in Table 2 were obtained from experimental data [2: Figure 10 and Table 1], assuming the NiCoCrAlY coating and CMSX-3 substrate are made up of Ni and Al exclusively. The results of solving Eq. 2 for $\tilde{D}$ are shown in Table 2 along with the initial concentrations of Ni and Al. The values obtained for $\tilde{D}$ after 4 hours of pre-diffusion at 1079 °C range from 1.6 E^{-11} to 2.0 E^{-12} (cm^2/sec) which agree with the diffusivity of 5.0 E^{-11} reported by Lee et.al. [9] for a 100 μm thick MCrAlY coated specimen subjected to isothermal oxidation at 1093 °C.

The second correlation involved plotting the concentration gradient data points obtained from two samples from [2], one which had 4 hours of diffusion bonding heat treatment and the other with an additional 100 hours of isothermal diffusion[1], on top of the predicted concentrations, shown in Figure 4.
A good fit is obtained with the 4 hr specimen data points, owing primarily to the fine microstructure still present in both the substrate and coating after the short diffusion time. The fit of the 100 hr specimen data also follows the predicted gradient on the substrate side, but appears to delineate from the gradient on the coating side. This

[1] The microprobe analysis data used for the 100 hour isothermal test was not available at the time of the second correlation. Therefore the data obtained from a 20 second heating, 60 second hold and 15 second cooling (6000 cycle test) specimen was used based on similar microstructures from SEM analyses

discrepancy arises due to the coarse microstructure in the coating after 100 hr of diffusion and the presence of Co or Cr precipitates, not accounted for in the binary analysis, which affect the relative Ni and Al concentration observed with the microprobe.

3.3 Predicted Gradients and Proposed Diffusion Time

A computer program was written (Appendix A.1) to solve Eq. 2 for different diffusion times. The resulting concentration gradient N_A and the concentration gradient dN_A/dx at the interface for times of 4 and 100 hours are shown in Figure 4 and Figure 5, respectively. To reduce the concentration gradient (with which to suppress internal (Kirkendall) void formation) by a factor of 4 over the 4 hour time tested by [2], a 60 hour pre-diffusion time was predicted (Fig. 5).

4 RESULTS AND DISCUSSION

4.1 Microstructure and Composition Identification Method

In order to determine the Ni and Al concentration gradients present in the specimens prior to thermal fatigue testing, two specimens were aged in a furnace for 60 hours at 1090 °C in air. One specimen (Spec. 2) was then mounted and ground down to its mid-plane, with a final polish of 0.3 μm using an alumina powder solution. The other specimen (Spec. 14) was fatigue tested prior to grinding and polishing. A Nikon optical microscope and a Cambridge scanning electron microscope operating at an accelerating potential of 20 kV were used to identify the resulting microstructure. For enhanced viewing under the microscopes the specimens were etched with a solution of 33% HNO_3, 33% HCl, 33% $C_3H_8O_3$ and

1% HF for 10 seconds. An additional polish with 0.3 μm alumina was then performed to remove the etched material (<10nm) prior to composition examination with a JOEL model 733 electron microprobe. The microprobe was operated at an accelerating potential of 15 kV, a beam current of 20 nA and a nominal beam diameter of 1 μm with a positioning accuracy of better than 0.5 μm. The coating and substrate composition were determined by measurement of the intensity of the spectral lines emitted from the K_α or L_α shells of their respective elements corrected by a ZAF (atomic number, absorption, fluorescence) program and compared to pure element standards of Ni, Co, Cr, Al, Mo, Ti, Ta, W, and Y.

4.2 Concentration Gradient Verification Specimen

4.2.1 Microstructure and Composition

The microstructure resulting in the specimen after 60 hours of aging is shown in the optical micrograph of Figure 6 and a backscattered electron micrograph in Figure 7, along with the results of the microprobe analysis (shown as a trace on the photo). The oscillation of the concentration in Figure 7 is due to the 1 μm beam diameter of the microprobe being small enough to analyze the individual grains of β and γ in the coating. Three distinct regions (as in 100 hour isothermal specimen SEM micrograph in [2]), depicted as Regions 1, 2, and 3, are shown in Figure 7 with Region 1 representing the NiCoCrAlY coating region, Region 2 the interdiffusion zone and Region 3 the γ–γ' CMSX-3 substrate region. The coating and substrate can both be represented on the ternary Ni-Al-Cr phase diagram shown in Figure 8 where equivalent quantities are used for Ni (Ni=Ni+Co) and Al (Al+Ti+Ta+Mo) based on similar atomic dimensions, ternary diagrams, and relative diffusion characteristics [2]. The 70 μm coating region (Region 1, Fig. 7) is

composed of $\beta - \gamma$ microstructure with β (NiAl) grains (Point 3, Fig. 8) on the order of 3-7 μm and a thin layer (<1μm) of aluminum oxide on the surface. The 20 μm interdiffusion zone (Region 2, Fig. 7) contains γ with 3-10 μm grains of β and refractory-rich precipitates of Ti, Ta, and W (previously in solution within the γ of the substrate). The substrate (Region 3, Fig. 7) was comprised entirely of γ–γ' (Point 1, Fig. 8). Precipitates in and near the interdiffusion zone are shown in Figure 9, along with their atomic composition.

4.2.2 Concentration Gradient Verification

The normalized concentration of aluminum (assuming the binary system of Ni and Al as in Section 3) in Spec. 2 is superimposed on the predicted concentration gradient through the interface in Figure 10. The concentration gradient obtained experimentally (3.0 at%/mm from Spec. 2) reduced the gradient of the 4 hr diffused specimen of Busso by a factor of 4 and shows a good correlation with the predicted gradient (2.5 at%/mm), considering the exponentially decaying nature of the gradient.

4.3 Thermally Fatigued Specimen

4.3.1 Microstructure and Composition

After 6000 thermal fatigue cycles the microstructure and composition (Figure 11) of the 60-hour diffused specimen differed from the non-diffused specimen tested by Busso and McClintock [2] in two respects; first, fewer (42 versus 64) internal voids formed, and second, these voids did not go on to form cracks through the substrate. As in the identically fatigued specimen of Busso and

McClintock three regions of varying microstructure are present within the coating and interdiffusion zone. The compositional trace (Fig. 11) of the specimen (Spec. 14) produced through the use of the microprobe shows a 15-20 μm β-deficient zone of γ near the surface overlaying a 40-50 μm γ - β region containing elongated β grains with nominal dimensions of 40 μm length and 15 μm width. Between the γ - β region of the coating and the γ - γ' substrate lies a 40 μm transition zone of γ, containing Kirkendall voids nucleating at the base of the receding β grains and extending towards the substrate.

4.3.2 Cracking Observations

The cracking observed in the 60-hour diffused specimen (Spec. 14) was in all instances related to existing (prior to diffusion treatment) surface pits. The surface pits along the entire periphery of the specimen were mapped prior to testing and were correlated to cracks before and after the specimen was ground down to its midplane for micrographic examination. A total of 11 surface-pit-initiated cracks penetrated the substrate with 1 crack of 2100 μm, 3 cracks ranging from 1100 μm to 1500 μm, and 7 cracks between 100 μm and 500 μm in depth. The largest of these were near the [100] direction which had coating strains of $\Delta\varepsilon^{mech} \cong 0.71\%$. These surface pits (with dimensions of 30-70 μm diameter and depth) formed during the EB-PVD coating process and under production circumstances of aircraft gas-turbine blades would be minimized through optimization of the EB-PVD and peening operations [10].

A typical internal (Kirkendall) void in the 60-hour specimen (Spec. 14) is shown in a secondary electron micrograph in Figure 12. This void (Fig. 12) was near the [100] direction with a coating strain of $\Delta\varepsilon^{mech} \cong 0.71\%$ and had the nearest

surface-pit-initiated crack (of 500 μm depth) circumferentially spaced over 4500 μm (35 °) away. The overall number of midplane voids observed was reduced from 64 voids in Busso and McClintock's specimen to 42 voids in the current specimen (Spec. 14), with voids arising throughout the perimeter ($\Delta\varepsilon^{mech} = 0.51\%$ to 0.71%). Of the 42 voids present none produced cracks into the substrate, or out to the surface, whereas, 3 of the 64 voids in Busso and McClintock's specimen produced cracks. Statistically, using a 95% confidence limit, 0 to 4 cracks could have occurred in Spec. 14 and 1 to 10 cracks could have occurred in the reference specimen. Assuming that the midplane is cutting through a random plane of voids, an approximate void spacing, L_v, can be obtained by using the total number of voids, V_t, a mean void diameter, d_m, and the total arc length, c, to calculate a linear fraction of voids, L_f:

$$L_f = \frac{V_t * d_m}{c}, \tag{4}$$

and then approximate the void spacing:

$$L_v \approx \frac{d_m}{\sqrt{L_f}}. \tag{5}$$

This translates to a mean void spacing increase from 110 μm for the specimen of [2] to 150 μm for Spec. 14, or a 36% void spacing increase.

5 CONCLUSIONS

1. As a result of 60 hours of pre-diffusion at 1090 °C the concentration gradient of Al was reduced by a factor of 4 through the coating/substrate interface.

The use of binary (Ni and Al) diffusion, constant diffusivity, analysis was sufficient in predicting (within 20% of experimental gradient) the desired gradient of 2.5 at%/mm, with 60 rather than 4 hr of pre-diffusion.

2. The increase in pre-diffusion time reduced internal (Kirkendall) void formation, increased the void spacing 36%, and eliminated crack propagation into the substrate from these voids. Since no-void induced cracks penetrated the substrate, the only benefits of increasing pre-diffusion time would be to decrease void formation. As shown through the diffusion analysis, any further decrease in concentration gradient, through which to decrease void nucleation, would come at the expense of much longer diffusion times (100 hours for a factor of 5 reduction in gradient). Attempts to significantly decrease (10 hour reduction) the pre-diffusion time would be precluded by the need to maintain a similar concentration gradient reduction factor in order to preclude void induced substrate cracking. A more detailed analysis might only be justified after actual hardware testing was performed, thus obtaining true service conditions for subsequent correlation.

3. Of the 33 surface pits present before thermal cycling, 11 produced cracks which penetrated the substrate. Under actual service conditions these surface pits can and should be minimized.

REFERENCES

[1] Holmes, J.W. and F.A. McClintock, The chemical and mechanical processes of thermal fatigue degradation of an aluminide coating, to be published in *Metallurgical Transactions*.

[2] Busso, E.P. and F.A. McClintock, Mechanisms of thermal fatigue degradation of an overlay coating, submitted to *Material Science and Engineering*.

[3] Holmes, J.W., F.A. McClintock, K.S. O'Hara, and M.E. Conners, Thermal fatigue testing of coated monocrystalline superalloys, *Low-Cycle Fatigue*, ASTM STP 942, H.D. Salomon, G.R.Halford, L.R. Kaisand, and B.N. Leis (eds.) 1987, pp.672-691.

[4] Busso, E.P. , *Thermal Fatigue of an Overlay Coating for Single Crystal Nickel-Base Superalloys*, M.S. Thesis, Dept. Mech. Engr., M.I.T., May 1987.

[5] Busso, E.P., Stress-Strain Histories in Coatings on Single Crystal Specimens of a Turbine Blade Alloy, to be published in *Journal of Solids and Structures*.

[6] Goebel, J.A. and F.S. Pettit, Hot corrosion of Co-based alloys, Report ARL TR75-0235, *Air Force Contract F33615-72-c-1757*, June 1975.

[7] Goward, G.W., Protective coatings for high temperature alloys, *Source Book on Materials for Elevated Temperature Applications*, ASM Engr. Bookshelf, E.F. Bradley (ed.) 1979, pp. 369-384.

[8] Reed-Hill, R.E., *Physical Metallurgy Principles*, 2nd ed., Brooks/Cole Engineering Series, 1973.

[9] Lee, E.Y., D.M. Chartier, R.R. Biederman, and R.D. Sisson Jr., Modelling the microstructural evolution and degradation of M-Cr-Al-Y coatings during high temperature oxidation, *Surface and Coatings Technology* **32** (1987), pp. 19-39.

[10] Wortman, D.J., Manager - Advanced Coatings, General Electric Aircraft Engine Group Evendale, Personal Communication, January 1989.

		Ni	Co	Cr	Mo	W	Ti	Al	Ta	Y
CMSX-3 Substrate (MAR-M-247 derivative)	Wt %	66 4	4.6	7.9	0.5	8	1	5.6	6	-
	At %	67.9	4 7	9.1	0.3	2.6	1.1	12.4	1 9	-
CMSX-3 constituent phases	γ - Wt %	61 1	7.3	18.8	0 9	9.4	0 4	2	0 1	-
	γ - At %	62 4	7 4	21.6	0.5	3	0 5	4 4	0.04	-
	γ' - Wt %	69	3 2	2	0.3	7.3	1.3	7 6	9.2	-
	γ' - At %	70 6	3 2	2 3	0 2	2.3	1 6	16 7	3 1	-
NiCoCrAlY coating	Wt %	49.3	19.7	15 9	-	-	-	12 7	-	<0 2
	At %	42 8	17.1	15 7	-	-	-	24 2	-	<0 05

Table 1. Chemical compositions of substrate and coating. (From [2]).

	Actual Data		Norm. to Ni,Al	
x (mm)	n_A (Al at.%)	n_B (Ni at.%)	$N_A(x,t)$ (Al at.%)	$\tilde{D}$ (cm^2/sec)
3	18 6	45.0	29	2 0 e-11
4	20 0	41.6	31	1.2 e-11
5	21.2	44.3	32	1 2 e-11
6	23 0	44 0	33	1 1 e-11
7	24 2	43 6	36	2 3 e-12
8	25 4	43 3	37	1.2 e-12
9	27 5	43.0	39	1.6 e-12

Table 2. Predicted diffusivities from Eq. 2 using concentrations and distances for the 4 hr diffused specimen from [2: Figure 10 and Table 1]. (N_A^1 = 0.154 and N_A^2 = 0.361).

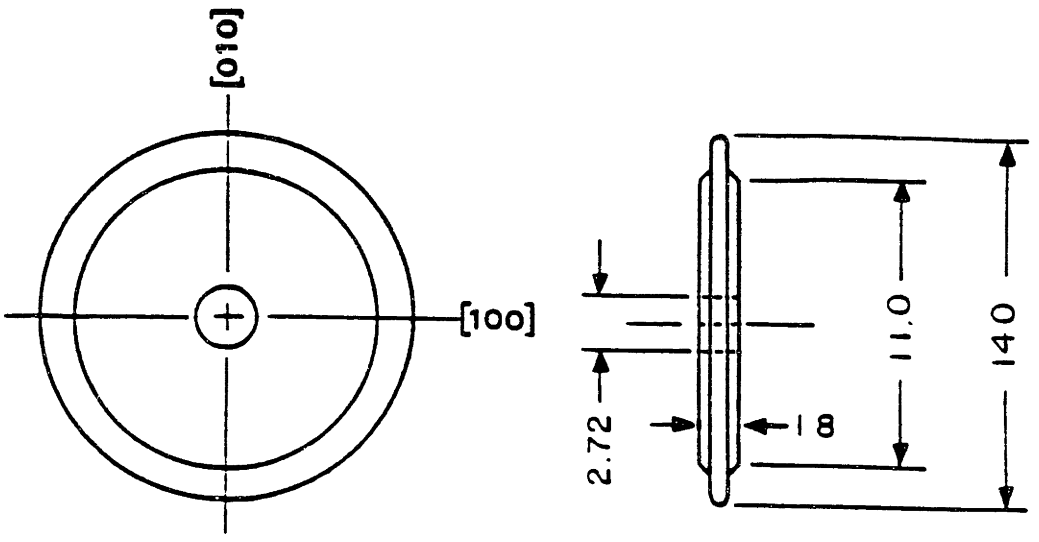

(a) Specimen geometry.

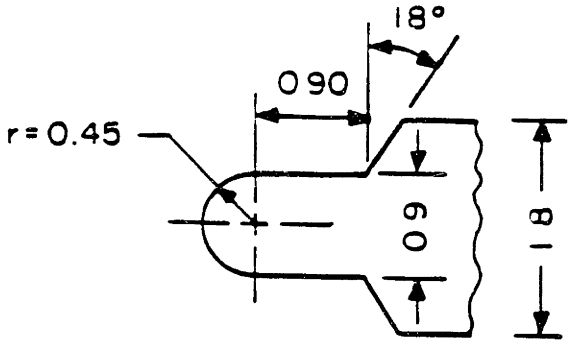

(b) Detail of specimen periphery.

Figure 1. Detailed geometry of stepped-disk specimen. (From [2] [3]). (Dimensions in mm).

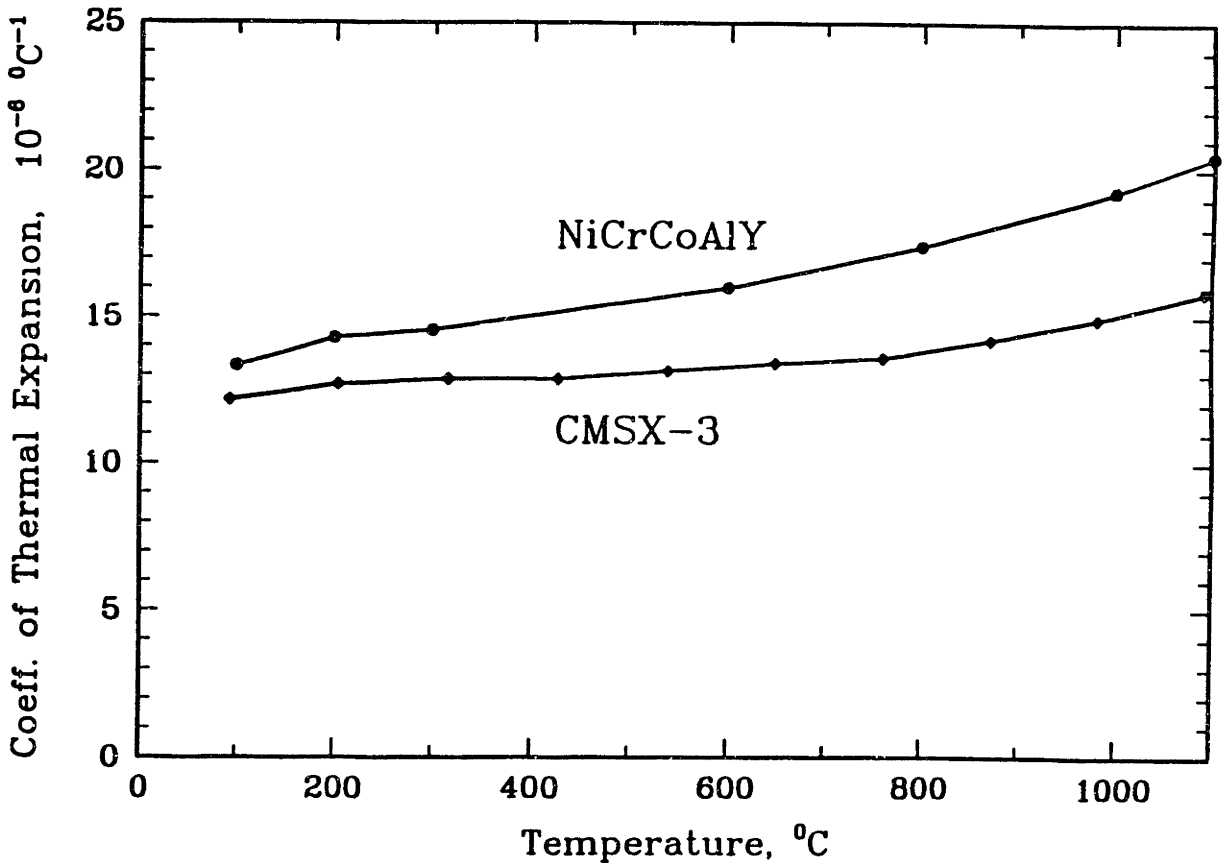

Figure 2. Coefficient of thermal expansion for the substrate (CMSX-3) and coating (NiCoCrAlY). (Reference temperature = 25 °C). From [2].

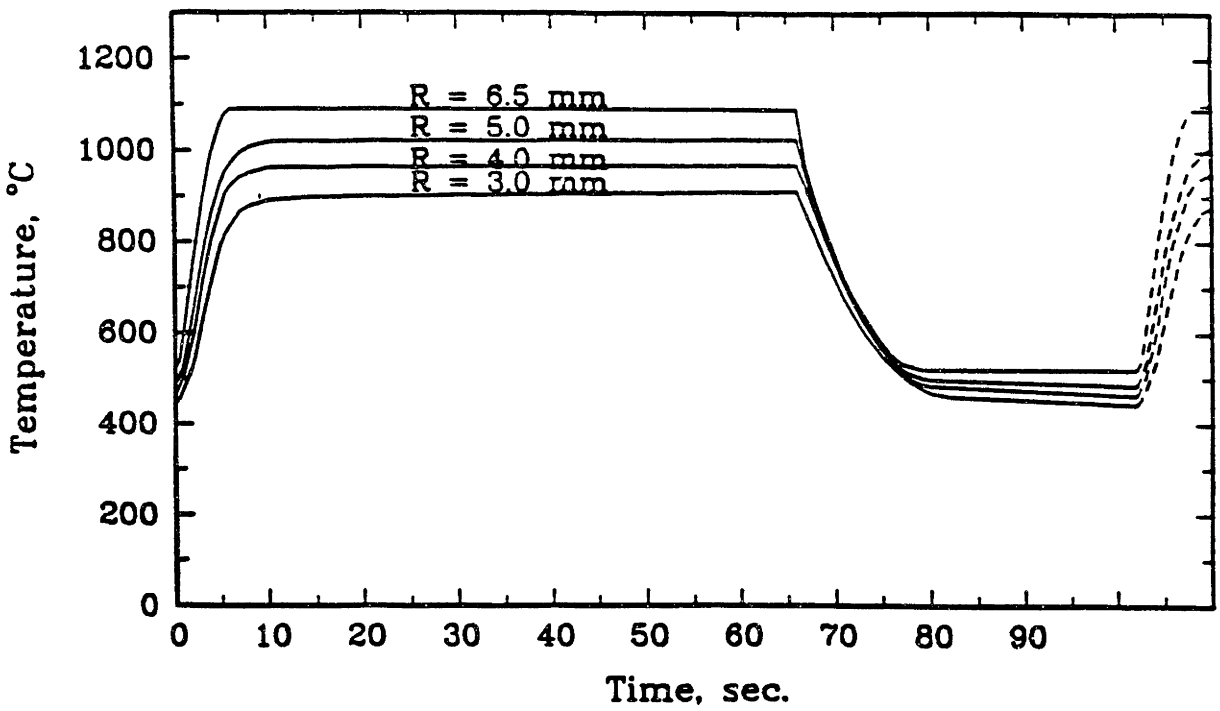

Figure 3. Radial temperature distribution in Spec. 14 when its periphery is cycled (6 sec. heat, 60 sec. hold, 15 sec. cool) from 520 °C to 1090 °C. From [2].

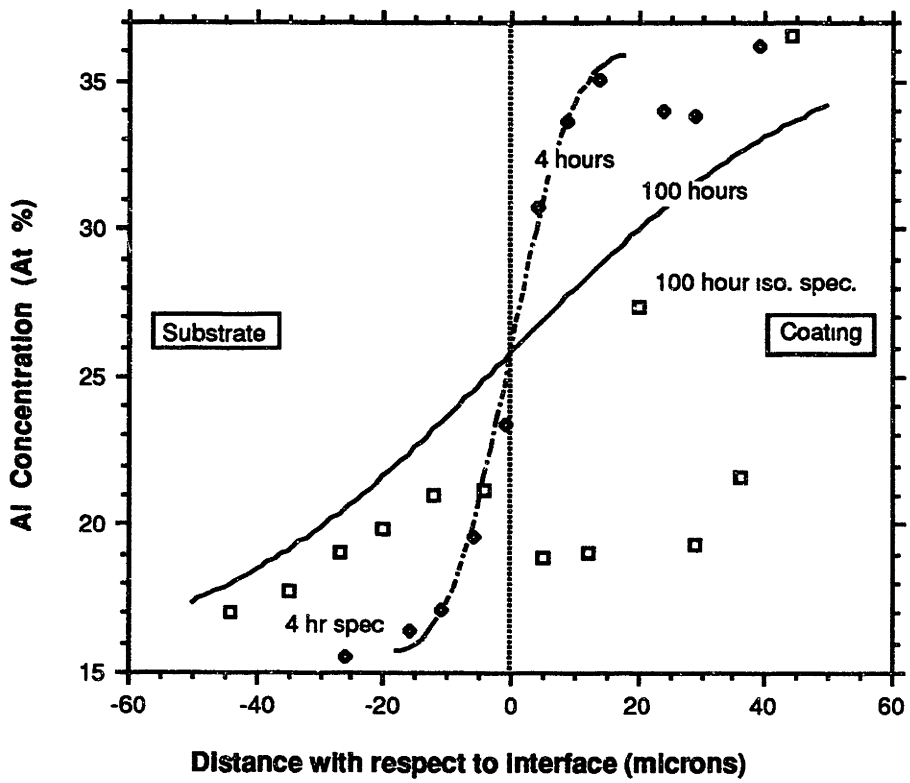

Figure 4. Predicted gradient compared with experimental data from [2].

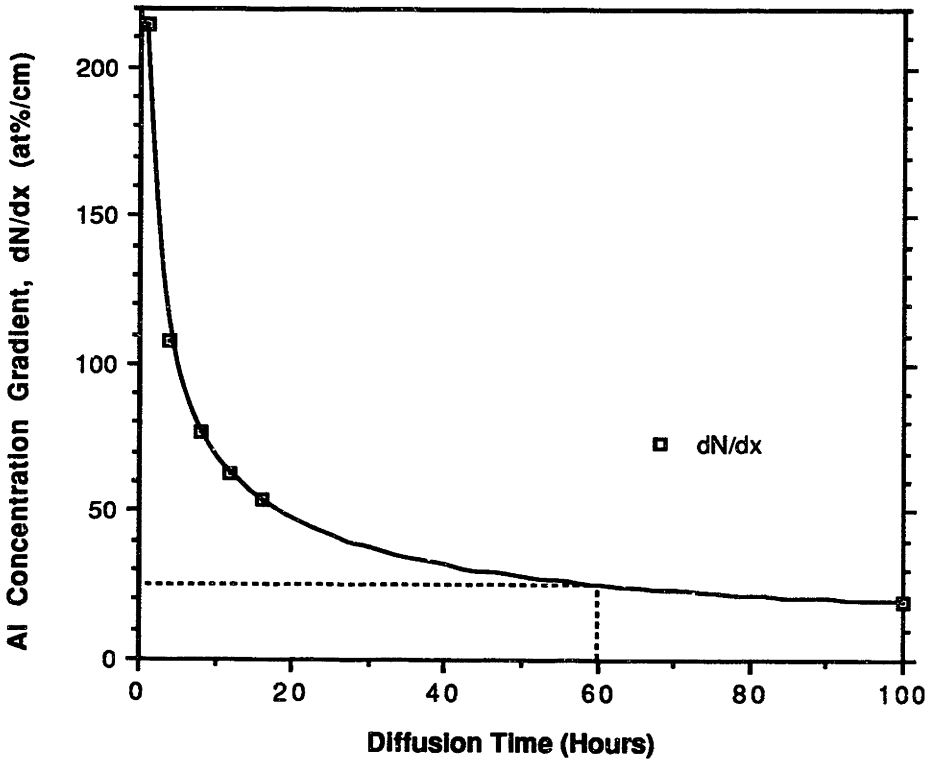

Figure 5. Predicted Al Concentration Gradient through the Coating/Substrate Interface.

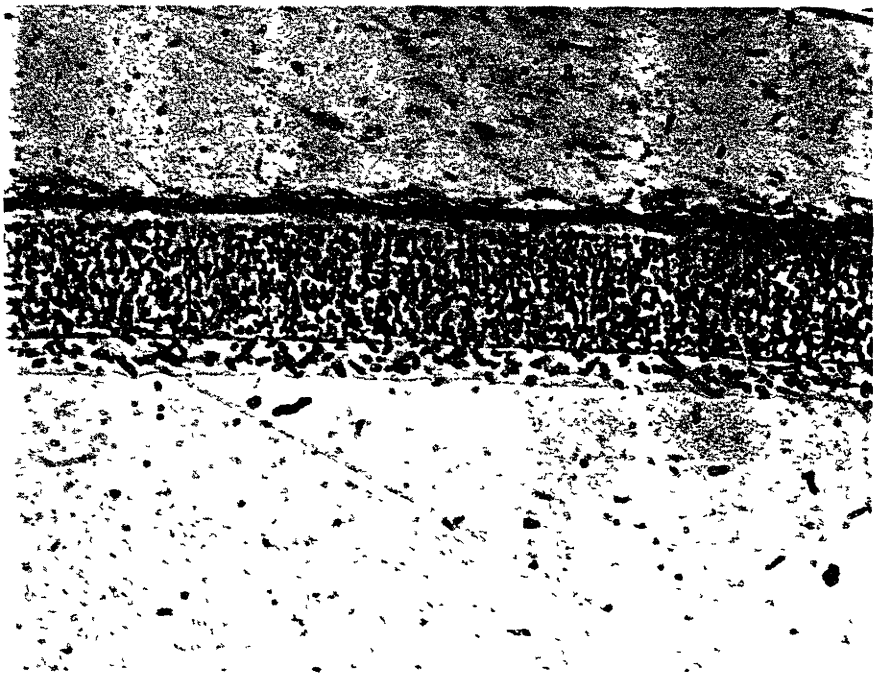

Figure 6. Optical microscope photograph (20x magnification) of 60-hour pre-diffusion specimen (Spec. 2). [100] direction.

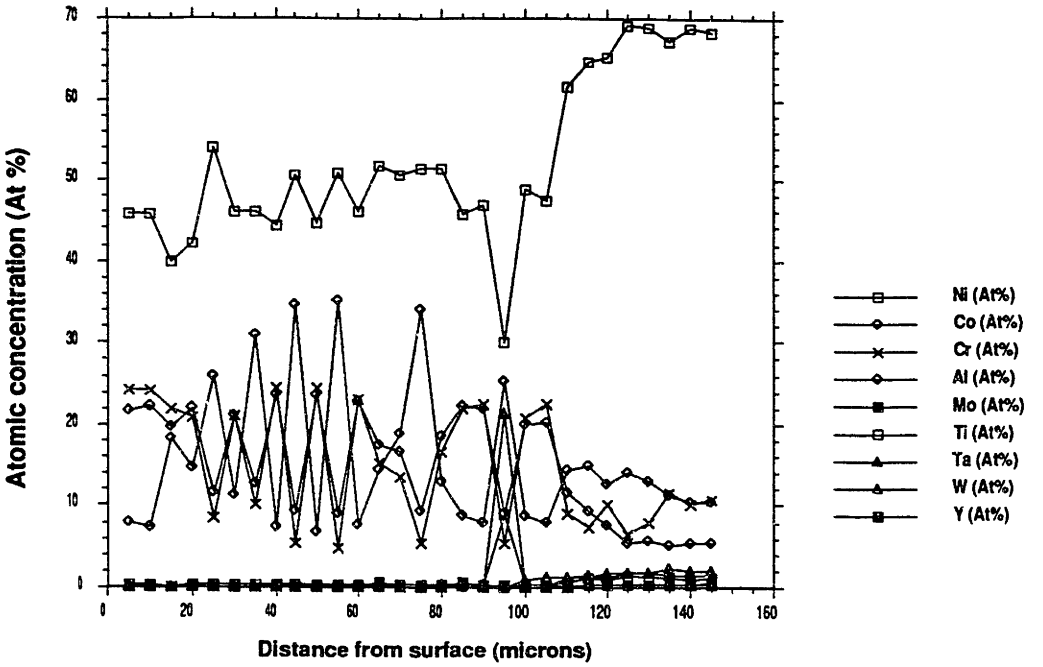

Spec. 2 atomic concentration of all substrate/coating constituents (from microprobe data). [100] direction

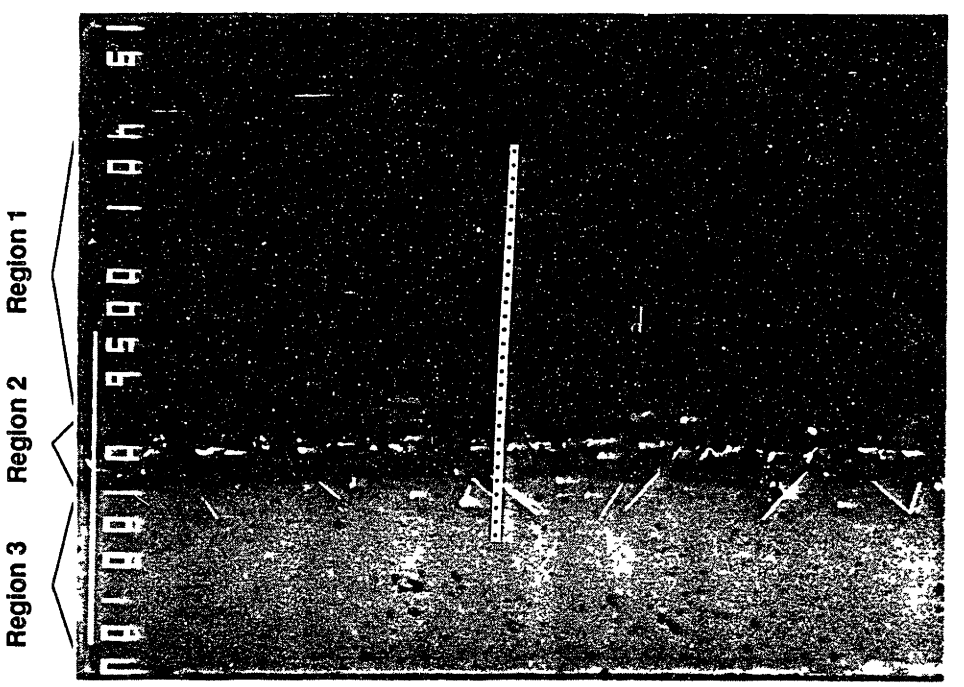

Figure 7. Backscattered electron micrograph and microprobe composition trace of Spec. 2 (60 hour diffusion). [100] direction.

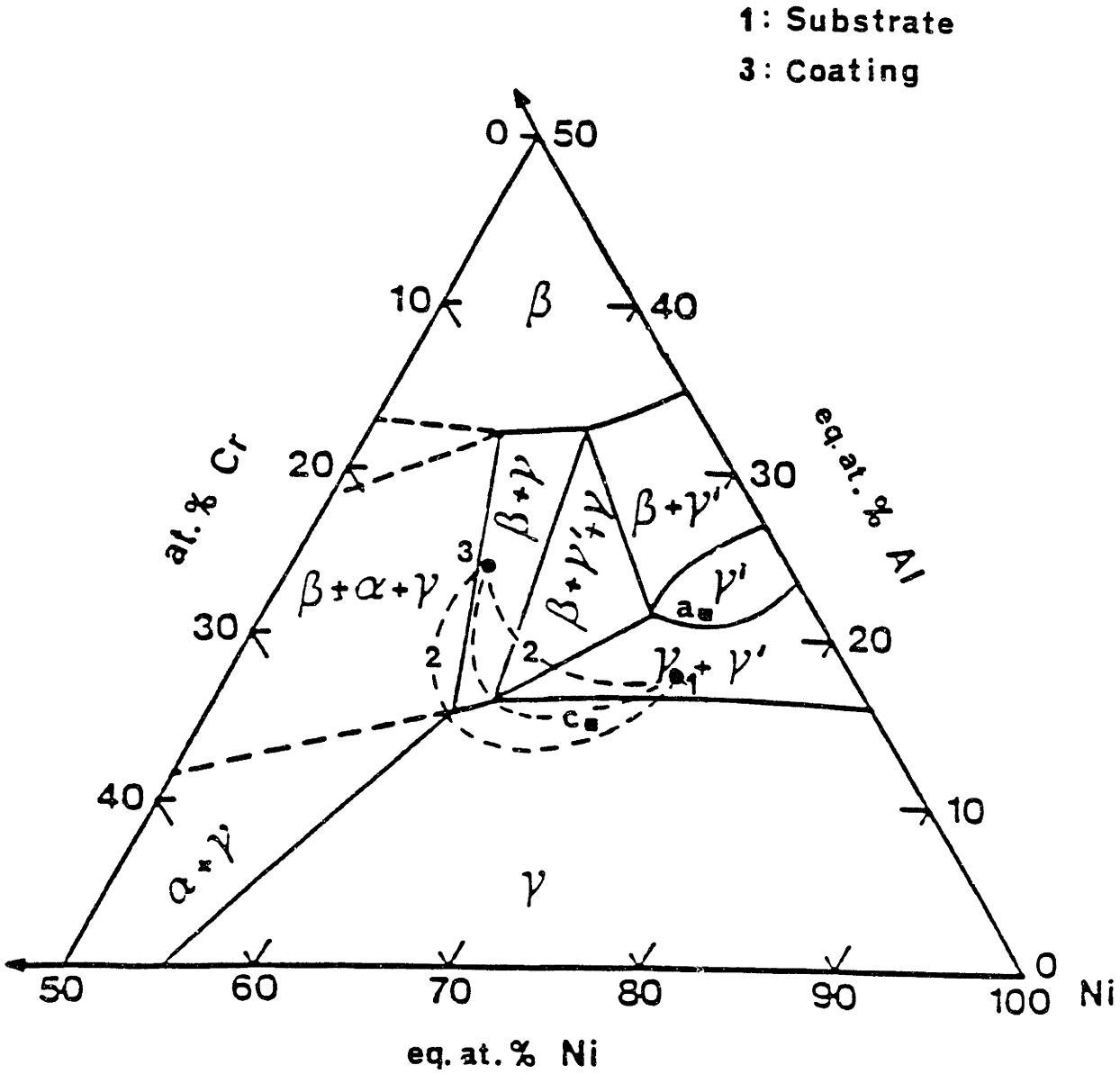

Figure 8. Ni-Cr-Al phase diagram at 1090 °C. From [1] [2].

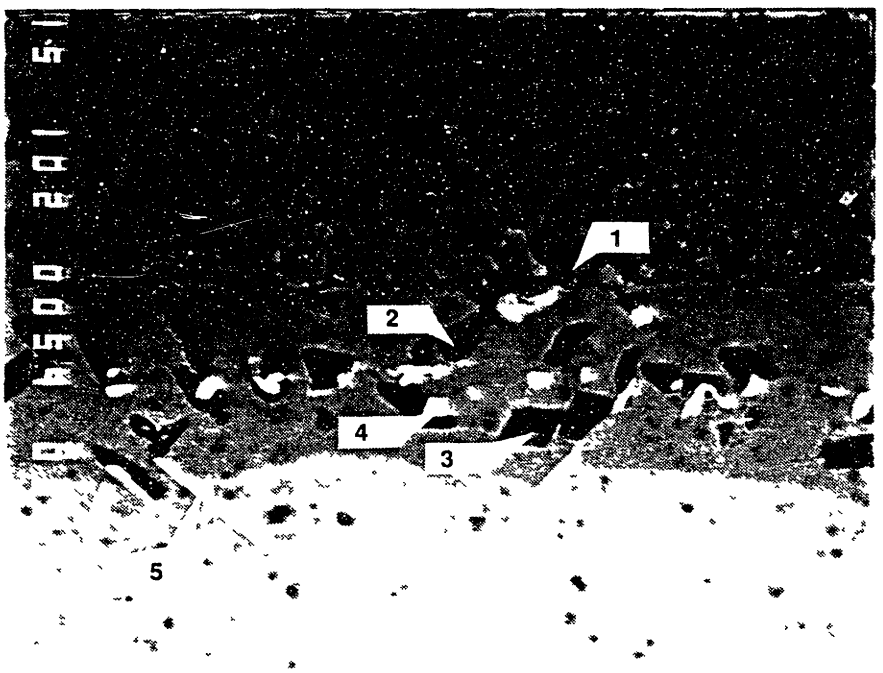

Element (At%)	Point 1	Point 2	Point 3	Point 4	Point 5
Ni	50 58	50 48	49 67	9 91	23 73
Co	9 44	9 32	8.58	3 73	12 68
Cr	5 54	5 61	5 52	2 91	23 17
Al	33 67	34 07	35 44	1 42	1 56
Mo	0 03	0 04	0 05	0 18	3 38
Ti	0 27	0 26	0 29	25 76	0 94
Ta	0 18	0 17	0 26	52 36	4 57
W	0 06	0 05	0 04	1 63	28 19
Y	0 23	0	0 15	2.11	1 78

Atomic composition of precipitates in the interdiffusion zone of Spec 2

Figure 9. Specific grain composition within the interdiffusion zone of the 60-hour diffusion specimen. [100] direction.

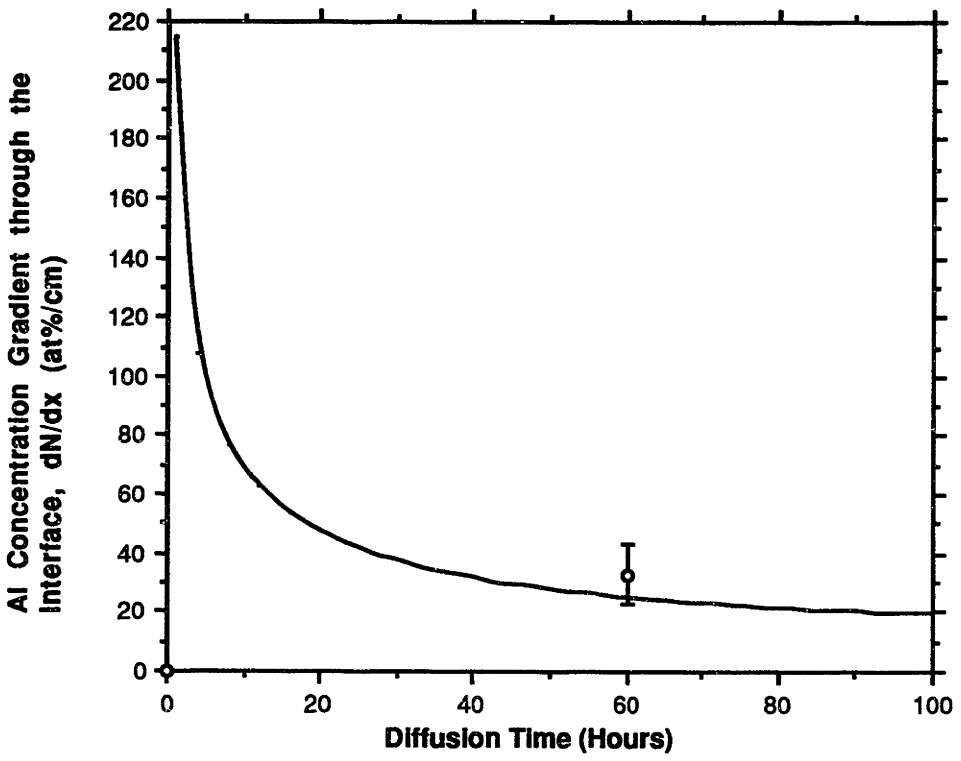

Figure 10. Correlation of Spec. 2 (Fig. 7) with predicted Al concentration gradient (averaged over 10 microns) through the coating/substrate interface.

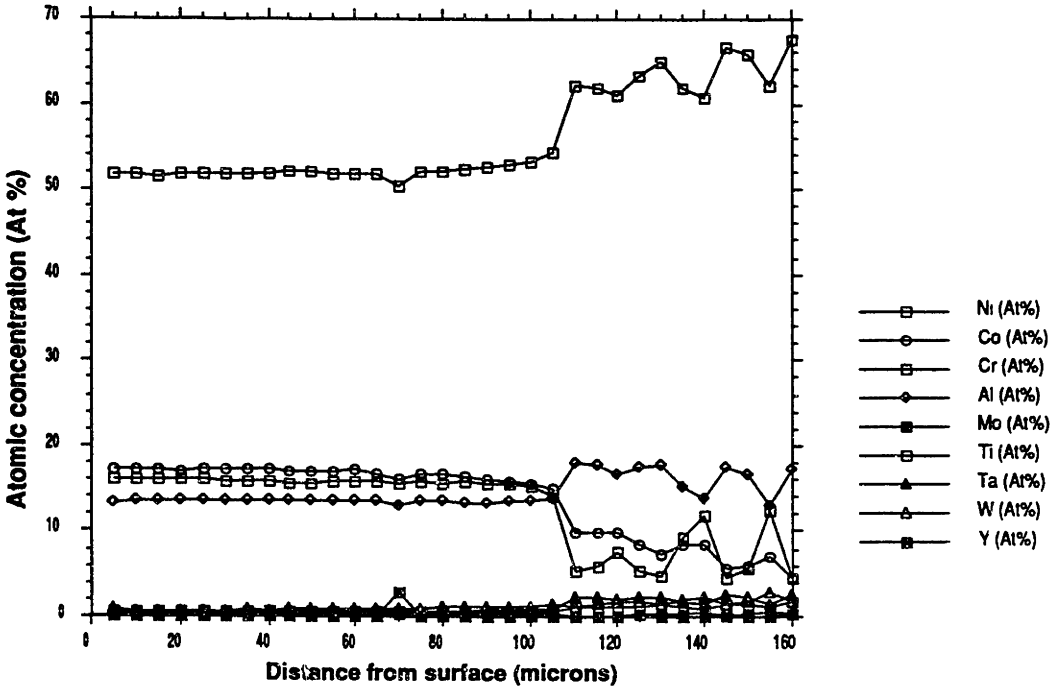

Specimen 14 atomic concentration of all substrate/coating constituents (from microprobe data). [100] direction.

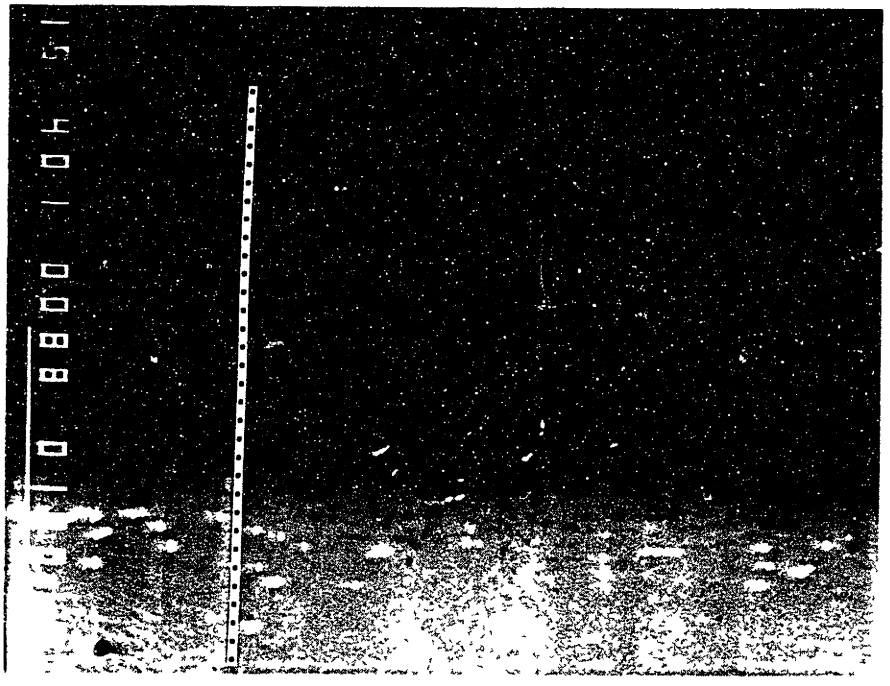

Figure 11. Backscattered electron micrograph and microprobe composition trace of Spec. 14 (Thermally fatigued). [100] direction.

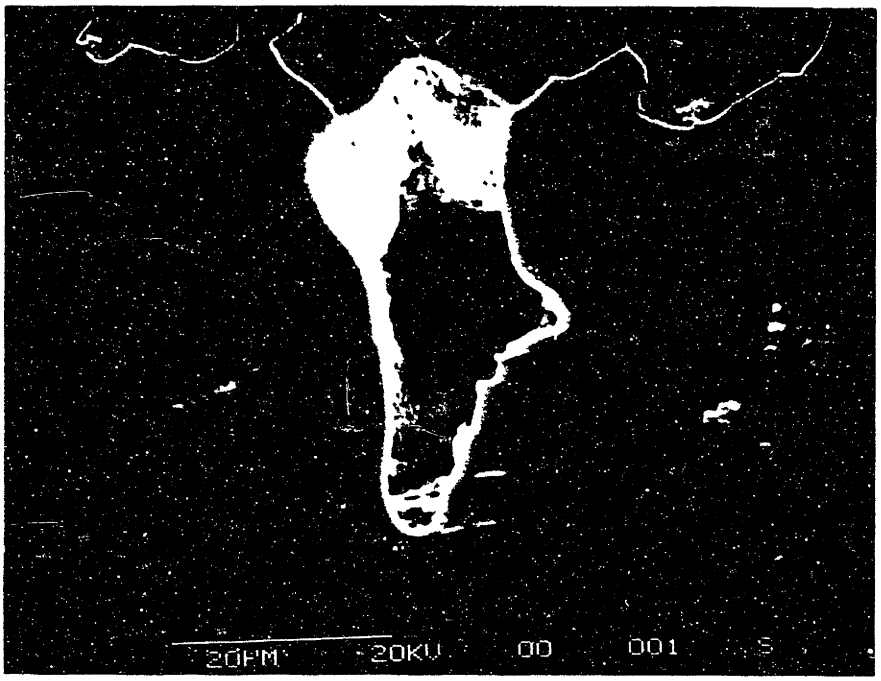

Figure 12. Secondary electron micrograph of an internal (Kirkendall) void in thermally fatigued specimen (Spec. 14). [100] direction.

A.1 BINARY DIFFUSION CONCENTRATION PREDICTION PROGRAM

```
C*****************************************************************
C
C       This program computes the concentration of one element A
C       in a binary system with two different A+B concentrations
C       with the following equation (Eq. 2 in the text, using A1 as N_A^1,
C       A2 as N_A^2, etc.):
C
C       AN=A1+((A2-A1)/2)*(1+ERF(X/(2SQRT(D*T))))
C
C*****************************************************************
        DIMENSION AN(110),ERF(110)
        OPEN (UNIT=2,FILE='FILE2')
        WRITE(2,110)
        WRITE(2,111)
        WRITE(2,112
        WRITE(2,113)
        WRITE(2,114)
        WRITE(2,115)
        WRITE(2,116)
        WRITE(2,117)
        WRITE(2,118)
        WRITE(2,119)
        WRITE(2,120)
        WRITE(2,110)
        WRITE(2,141)
        WRITE(2,142)
        WRITE(2,143)
        DO 101 J=1,100,99
                PRINT*,('J='),J
C
C               T=DIFFUSION TIME (SECONDS)
C
                T=FLOAT(J)*3600
                PRINT*,('T='),T
                WRITE(2,130)
                WRITE(2,131)
                DO 100 I=1,101
                        PRINT*,('I='),I
C
C       X=DISTANCE FROM INTERFACE (CENTIMETERS)
C
                        X=(FLOAT(I)-51.)10000
C
C       A1=ATOMIC FRACTION OF A IN A+B ON SIDE 1
C
                        A1=0.154
C
C       A2=ATOMIC FRACTION OF A IN A+B ON SIDE 2
C
```

```
                    A2=0.361
                    PRINT*,('A2='),A2
C
C       D=DIFFUSIVITY OF A+B (CM**2/SEC.)
C
                    D=2E-11
                    PRINT*,('D='),D
                    Y=X/((2*SQRT(D*T)))
                    PRINT *,('Y='),Y
                    C=2/SQRT(3.1415927)
                    T1=Y
                    T2=(Y**3)/3
                    T3=(Y**5)/10
                    T4=(Y**7)/42
                    T5=(Y**9)/216
                    T6=(Y**11)/1320
                    T7=(Y**13)/9360
                    T8=(Y**15)/75600
                    ERF(I)=C*(T1-T2+T3-T4+T5-T6+T7-T8)
C
C       AN(I)=CONCENTRATION OF A AT DISTANCE X AT TIME T
C
                    AN(I)=A1+((A2-A1)/2)*(1+ERF(I))
                    WRITE(2,150) X,AN(I)
                    PRINT*,X,AN(I)
 100          CONTINUE
 101    CONTINUE
 130    FORMAT('TIME T=')
 131    FORMAT(F12.1)
 150    FORMAT(F6.4,5X,F6.4)
 110    FORMAT('_____')
 112    FORMAT('FILE:  DIFF.F77  ')
 113    FORMAT('Concentration of A in a mixture of two A+B alloys')
 114    FORMAT('at a distance x from their interface at time t')
 115    FORMAT(' ')
 116    FORMAT('Concentration equation:')
 117    FORMAT(' ')
 118    FORMAT('AN=A1+((A2-A1)/2*(1+ERF(X/(2*SQRT(D*T)))')
 119    FORMAT(' ')
 120    FORMAT('_____')
 141    FORMAT(' ')
 142    FORMAT('x  (cm)       A1 ')
 143    FORMAT(' ')
        END
```